

Tailoring the ground state of the ferrimagnet $\text{La}_2\text{Ni}(\text{Ni}_{1/3}\text{Sb}_{2/3})\text{O}_6$

D. G. Franco^{a,b}, R. E. Carbonio^b, E. E. Kaul^{a,c}, G. Nieva^{a,c}

^a*Laboratorio de Bajas Temperaturas, Centro Atómico Bariloche - CNEA, 8400 Bariloche, Río Negro, Argentina.*

^b*INFIQC-CONICET, Depto. de Físico Química, Facultad de Ciencias Químicas, Universidad Nacional de Córdoba, Ciudad Universitaria, X5000HUA Córdoba, Argentina.*

^c*Instituto Balseiro, CNEA and Universidad Nacional de Cuyo, 8400 Bariloche, Río Negro, Argentina.*

Abstract

We report on the magnetic and structural properties of $\text{La}_2\text{Ni}(\text{Ni}_{1/3}\text{Sb}_{2/3})\text{O}_6$ in polycrystal, single crystal and thin film samples. We found that this material is a ferrimagnet ($T_c \approx 100$ K) which possesses a very distinctive and uncommon feature in its virgin curve of the hysteresis loops. We observe that below 20 K it lies outside the hysteresis cycle, and this feature was found to be an indication of a microscopically irreversible process possibly involving the interplay of competing antiferromagnetic interactions that hinder the initial movement of domain walls. This initial magnetic state is overcome by applying a temperature dependent characteristic field. Above this field, an isothermal magnetic demagnetization of the samples yield a ground state different from the initial thermally demagnetized one.

Keywords: Ferrimagnetics, Doubleperovskites, Magnetic frustration, Superexchange and super-superexchange interactions, Magnetic oxides

1. Introduction

The physics and chemistry of complex oxides have been largely studied due to the rich phenomena resulting from their combined magnetic, charge and orbital degrees of freedom. Among these complex oxides, those with

Email address: gnieva@cab.cnea.gov.ar (G. Nieva)

perovskite structure ABO_3 have been extensively studied. They are the archetype of superconducting oxides, giant magnetoresistive oxides and the materials for the emergent field of novel device functions [1].

The size and oxidation state of A and B cations determine the symmetry of the perovskite structure, that departs from cubic when a tilting of the octahedral arrangement of oxygen around the B cation occurs [2]. Also, the partial replacement of A or B site cations by isovalent or aliovalent A' and B' atoms could result in a double perovskite structure with lower symmetry. In double perovskites with general formula $A_2(BB')O_6$, B and B' atoms occupy two different crystallographic sites, and an ordered or disordered occupancy of them depends on the oxidation state and size difference between B and B' ions [3, 4].

Many of the magnetic interactions found in transition metal oxide perovskites are due to superexchange and/or super-superexchange interactions mediated through the oxygen orbitals. In some materials the relative strength and arrangement of these interactions determine the magnetic structure, range of the ordering temperatures and the possibility of frustration [5, 6, 7, 8, 9]. In particular, the effective spin lattice, ferro- or antiferromagnetic interactions among transition metal ions, depends on a delicate balance provided by the charge in the linking orbital, the bond angle, the degree of orbital overlap, the distance between interacting ions and their spin state [10, 11]. In the specific case of the perovskite structure, the typical bond angles and distances usually favors antiferromagnetic superexchange interactions [11]. However, in some particular cases, when there are more than one electronic pathway in the linking orbitals, a destructive interference leads to the cancellation of the antiferromagnetic interaction. In these cases, a weak ferromagnetic coupling becomes relevant [12].

In transition metal oxides, the competing effects of a ferromagnetic interaction and local frustration leads to a spin glass like behavior [13]. The main signatures of this frustration are made evident in the time evolution from metastable magnetic states [14]. However, in bulk ferro/ferrimagnetic samples, a local frustration is normally hard to visualize due to the magnetic history dependence of the metastable states created by the pinning of domain walls.

Also in some transition metal oxides the competition between a ferro- and antiferromagnetic ground states leads to a nonequilibrium glassy behavior that arises from a kinetic arrest of a ferromagnetic to antiferromagnetic phase transition [15]. These materials are identified as magnetic glasses [16]

consisting of ferro- (or ferri-) magnetic and antiferromagnetic clusters frozen randomly with a dynamics similar to that of structural glasses.

This article will present a detailed magnetic study of the ferrimagnetic double perovskite $\text{La}_2\text{Ni}(\text{Ni}_{1/3}\text{Sb}_{2/3})\text{O}_6$ [17, 18] showing evidence of a frustrated magnetic state at low temperatures. The properties of this compound were explored using polycrystalline, single crystalline and thin film samples. The main result is the observation that below 20 K there is evidence of a microscopically irreversible process involving the interplay of competing antiferromagnetic interactions that hinders the initial magnetic polarization or the movement of domain walls and determines the microscopic nature of the strong pinning centers found in this system [19]. This material results in a model system for studying the seldom found ferrimagnetic Ni^{2+} oxides and the low temperature glassy or magnetically disordered state present in many complex transition metal oxides.

2. Experimental details

We prepared polycrystalline samples of $\text{La}_2\text{Ni}(\text{Ni}_{1/3}\text{Sb}_{2/3})\text{O}_6$ by conventional solid-state reaction. Stoichiometric amounts of La_2O_3 , $\text{Ni}(\text{NO}_3)_2 \cdot 6\text{H}_2\text{O}$ and Sb_2O_3 were ground and fired at 1400°C for 12 hours in air. The single crystals were grown by the floating zone technique in a double ellipsoidal mirror furnace. The thin films were grown using RF magnetron sputtering in an Ar/O_2 atmosphere on (100) SrTiO_3 substrates at $700\text{-}800^\circ\text{C}$. We checked the composition of all the investigated samples by EDS. Only the thin films showed a 10% Ni^{2+} deficiency not present in the stoichiometric target material. We carried out the structural analysis using powder X-ray diffraction (XRD) at room temperature. The magnetic measurements were performed in an QD-MPMS SQUID magnetometer in the range 2 to 300 K and -5 to 5 Tesla.

3. Results

3.1. Structural characterization

In spite of an earlier report of this structure as being orthorhombic [17], with a fully disordered arrangement of Ni^{2+} and Sb^{5+} ions, we found the crystalline symmetry to be monoclinic (space group $\text{P}2_1/\text{n}$) with a rock salt arrangement of BO_6 and $\text{B}'\text{O}_6$ octahedra described by the $\text{a}^-\text{b}^-\text{c}^+$ system of three octahedral tilts in the Glazer's notation. The $(\text{Ni}^{2+}/\text{Sb}^{5+})_{2d}\text{O}_6$ and

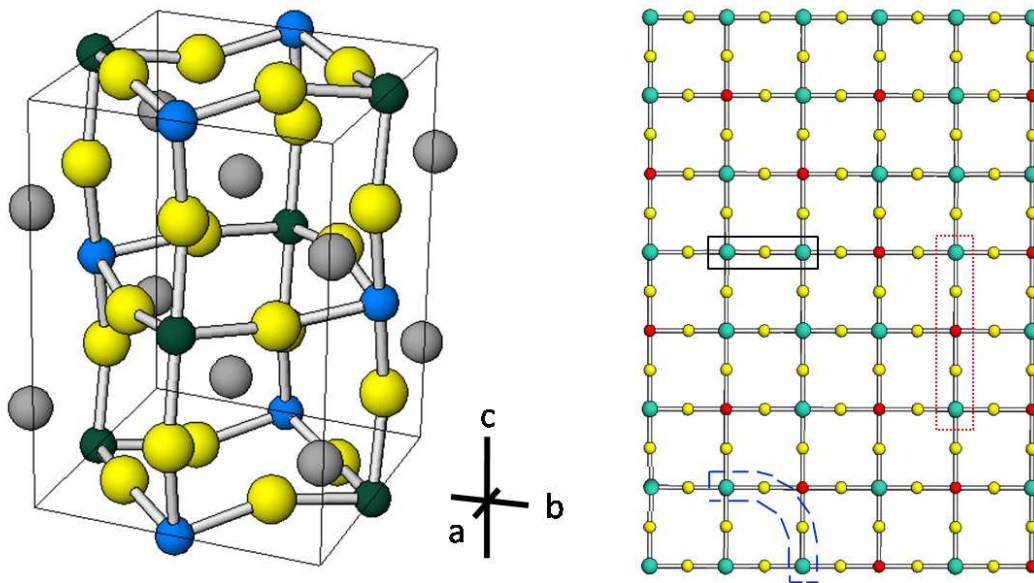


Figure 1: (color online) Left: monoclinic structure of $\text{La}_2\text{Ni}(\text{Ni}_{1/3}\text{Sb}_{2/3})\text{O}_6$ double perovskite. Grey spheres: La^{3+} , yellow spheres: O^{2-} , light blue spheres: B_{2d} ions and green spheres: B_{2c} ions. Right: two dimensional scheme of the distribution of B ions over the $2d$ and $2c$ sites for $\text{La}_2(\text{Ni})_{2d}(\text{Ni}_{1/3}\text{Sb}_{2/3})_{2c}\text{O}_6$ showing the different neighbors of the magnetic Ni^{2+} ions (turquoise spheres): first next nearest neighbors (1 nn, black), second next nearest neighbors (2 nn, dash blue line) and third next nearest neighbors (3 nn, red dot line). Red spheres are Sb^{5+} ions and yellow spheres O^{2-} ions. For simplicity a square structure was supposed and lanthanum ions were omitted.

$(\text{Ni}^{2+}/\text{Sb}^{5+})_{2c}\text{O}_6$ octahedra are rotated in phase along the primitive c axis and out-of phase along the primitive a and b axes. We performed a Rietveld refinement of the structure using the FULLPROF program [20], obtaining the lattice parameters $a = 5.6051(3)$ Å, $b = 5.6362(3)$ Å, $c = 7.9350(5)$ Å and $\beta = 89.986(4)^\circ$. The occupancy of the two crystallographic sites $2d$ and $2c$ were refined allowing the $\text{Ni}^{2+}/\text{Sb}^{5+}$ distribution to vary, in order to model the octahedral site disorder. We found that the $2d$ cation site is almost fully occupied by Ni^{2+} while the $2c$ site has an occupancy close to $1/3$ of Ni^{2+} ions and $2/3$ of Sb^{5+} . The resulting crystallographic formula can be written as $\text{La}_2(\text{Ni}_{0.976}\text{Sb}_{0.024})_{2d}(\text{Ni}_{0.357}\text{Sb}_{0.643})_{2c}\text{O}_6$. It should be noted here that this space group does not allow a further ordering of the Ni^{2+} and Sb^{5+} ions at $2c$ site. Figure 1 shows the structure of $\text{La}_2\text{Ni}(\text{Ni}_{1/3}\text{Sb}_{2/3})\text{O}_6$ and also a schematic two dimensional square view of $\text{Ni}^{2+}/\text{Sb}^{5+}$ distribution among $2d$ and $2c$ sites. From this picture it can be seen that Ni^{2+} ions have three

types of Ni^{2+} neighbors: first next nearest neighbors (mediated by -O-, that is, superexchange), second next nearest neighbors (through a -O-O- bridge) and third next nearest neighbors (-O-Sb⁵⁺-O-, super-superexchange).

Small crystals with a face parallel to the (103) planes could be extracted from the rod grown in the mirror furnace. The rocking curve on the (103) peak had a FWHM = 0.25° and the interplanar spacing showed a 0.05% reduction with respect to the bulk.

The thin films (100 -130 nm thick) were grown epitaxially in the *c*-axis direction. From XRD we measured a 1.4% *c*-axis expansion as compared with bulk samples, considering a constant cell volume. This corresponds to a 1.5% ($\text{Ni}^{2+}/\text{Sb}^{5+}$)_{2*d*}-($\text{Ni}^{2+}/\text{Sb}^{5+}$)_{2*c*} distance reduction in the *ab*-plane, to match the Ti-Ti distance of the substrate. Rocking curves showed typically a FWHM = 0.4° indicating a good crystallographic quality of the $\text{La}_2\text{Ni}(\text{Ni}_{1/3}\text{Sb}_{2/3})\text{O}_6$ films.

3.2. Magnetic characterization

We measured the magnetization as a function of temperature (*M* vs *T*) using a ZFC-FC procedure (i.e. cooling with zero applied field or with a finite applied field) for several powder samples, thin films and single crystals. The lower curve in Figure 2(a) (open diamonds) shows a typical result for polycrystalline samples with a Curie-Weiss behavior at high temperature, $\frac{M}{H} = \frac{C}{T-T_{CW}}$, with *C* the Curie constant and *T*_{CW} the Curie-Weiss temperature. The lower inset in Figure 2(a) shows the magnetization derivative *dM/dT* used to determine the transition temperature to the ordered state, the Curie temperature, *T*_C. A Curie-Weiss fit of several polycrystalline samples gives *T*_{CW} = 155(6) K and *T*_C = 98(2) K. The effective magnetic moment, calculated from the Curie constant is *p* = 2.3(1) μ_B . This value is lower but close to the one expected for spin only Ni^{2+} , *p* = 2.86 μ_B .

A typical result for the single crystals is also shown in Figure 2(a), filled circles. In this case *T*_{CW} = 138(4) K and *p* = 2.60(4) μ_B . We measured the single crystals with the magnetic field applied along two crystallographic directions, *H* || (103) and *H* || (010). In the upper inset of Figure 2(a) the susceptibility extracted from magnetization measurements at 1 and 5 kOe ($\Delta M/\Delta H = (M(5 \text{ kOe}) - M(1 \text{ kOe}))/4 \text{ kOe}$) is shown. The inflection point of these curves, identified with *T*_C, is located at 105 K which agrees very well with the polycrystalline samples.

The thin films paramagnetic behavior (*T* > *T*_c) is very difficult to isolate from the total signal, given their small mass, typically about 40 μg . How-

ever, subtracting the substrate magnetization contribution, a clear transition to a ferromagnetic state could be observed. Figure 2(b) shows the FC magnetization at 1 kOe, applied parallel to the surface of the film ($H \perp (001)$). The low temperature signal is approximately three times smaller than the one observed on the polycrystals and single crystals. The inset in Figure 2(b) shows dM/dT , the peak indicates a $T_C = 78$ K, which is about 20 % smaller than for bulk samples.

Hysteresis loops (M vs H) were measured at several temperatures for $T < T_c$. Figure 3 shows typical loops at $T = 2$ K for a thin film, a single crystal and a polycrystalline pellet. For the crystals, loops with the applied field along the (103) and (010) directions are included (Figure 3(c)). In this case the initial magnetization branch, the M vs H virgin curve measured after cooling at zero field, falls always outside the loop area for temperatures below about 20 K. This effect can be interpreted as a sign of frustration, is less visible in pellets and was not observed in films.

For temperatures below 20 K, we also measured the hysteresis loops after cooling the sample in 1 T, observing that they coincide with those measured after ZFC. No shift was found in the coercive fields ruling out the presence of exchange bias [21].

4. Discussion

4.1. The ordered state

The value of the Curie-Weiss constant, the shape of the M vs H curves and the hysteretic behavior, all point to a ferromagnetic state of the Ni^{2+} below 100 K. However, the saturation magnetization value, M_s , taken as the asymptotic extrapolation with a Langevin function of the behavior at the largest applied field (5 T), has a lower value than the one expected for the ferromagnetic complete polarization of the Ni^{2+} magnetic moments, $2.67 \mu_B/\text{f.u.}$. The experimental M_s values range from $0.73 \mu_B/\text{f.u.}$ to $1.19 \mu_B/\text{f.u.}$ considering films, single crystals and polycrystalline samples. These smaller experimental values are better understood if the system behaves as a ferrimagnet having two Ni^{2+} magnetic sublattices antiferromagnetically coupled, one at the $2d$ and another at the $2c$ sites. The near $1/3 \text{ Ni}^{2+}$ random occupation of the $2c$ sites sublattice give as a result uncompensated Ni^{2+} magnetic moments that order at 100 K. For a perfectly stoichiometric sample and full Ni^{2+} occupancy of the $2d$ site M_s should be $1.33 \mu_B/\text{f.u.}$, and lower values are expected if Sb^{5+} partially occupies also the $2d$ site. In particular, for

the refined occupancy of the octahedral sites in the powder, we can calculate $M_s = 1.24 \mu_B/\text{f.u.}$, close to the measured values. A similar ferrimagnetic order was reported in $\text{Sr}_2\text{Fe}(\text{Fe}_{1/3}\text{Mo}_{2/3})\text{O}_6$ [23] and $\text{Sr}_2\text{Fe}(\text{Fe}_{1/3}\text{U}_{2/3})\text{O}_6$ [22] where the magnetic Fe^{3+} ions and non magnetic Mo^{6+} or U^{6+} display a similar structural arrangement and magnetic array as the Ni^{2+} and Sb^{5+} in our case.

In order to get a microscopic understanding of the uncommon features seen in the virgin curves we shall analyze with some detail the characteristics of the ordered state through a study of the irreversible magnetization measurements from hysteresis loops. Figure 4 (a) shows that the coercive field for the single crystals (measured along the (103) direction) has a similar temperature behavior as that of the polycrystalline pellet at low temperatures [19]. We have previously established that the polycrystalline material coercive field has an upturn at $T \approx 20$ K changing from a weak domain wall pinning (WDWP) behavior at high temperatures to a strong domain wall pinning (SDWP) one below 20 K [19]. Analyzing the coercive field and the time dependence of the magnetization we have ruled out the freezing of large particles as a possible mechanism for the H_c upturn [19]. We found that in the single crystals the coercivity above 30 K is negligibly small. The film coercivity, measured at 2 K, is close to the bulk value, in spite of the expected H_c enhancement due to barriers for the DW motion introduced by surface roughness or local strains [25]. Figure 4(b) shows the T dependences of the the ratio between remanent and saturation magnetizations (M_r/M_s). This ratio and H_c increase steeply when the temperature is lowered below 20 K indicating increase in the energy needed to change the direction of M .

In the low temperature regime, $T \lesssim 20$ K, the polycrystalline pellets and single crystals ($H \parallel 103$) H_c data can be described by a model of strong domain wall pinning (SDWP),

$$H_c = H_{0S} \left[1 - \left(\frac{75k_B T}{4bf} \right)^{2/3} \right]^2 \quad (1)$$

where H_{0S} is the coercive field at zero temperature, f is the magnetic force needed to depin a domain wall and b is a measure of the domain wall thickness. The fitted values are shown in Table 1.

An estimation of b from the exchange stiffness, A , and anisotropy constant, K_1 , yield a small value of the domain wall thickness $b = \pi \left(\frac{2A}{K_1} \right)^{1/2} \simeq 10nm$. The anisotropy constant was calculated at 2 K from the area between

Table 1: Fitted parameters for the SDWP model below 20 K, for polycrystalline, *PC*, and single crystalline, *SC*, samples.

	$4bf$ (10^{-13} erg)	H_{0S} (Oe)
<i>PC</i>	3.07	780
<i>SC</i>	2.54	1440

the anhysteretic curves M vs H and the M axis [24] for the single crystals measured in the (103) and (010) direction. The value obtained was $K_1 = 3 \cdot 10^5$ erg/cm³¹. Although the calculated anisotropy constant is of the order of the value found in other ferrimagnets [24], the exchange stiffness constant is small due to the rather long average distance between uncompensated Ni²⁺ moments in the structure.

The microscopic origin of the change of regime of domain wall pinning mechanism at 20 K remains unclear. The onset of a disordered or frustrated magnetic state may result in the emergence of strong pinning sites for DW movement. The answer could be made evident analyzing the virgin curve in the hysteresis loops. The initial branch of the M vs H curve (cooling from above T_c at zero applied field) does not fall entirely within the magnetization loop for all the samples, except for the thin film, see Figure 3. In what follows this uncommon behavior will be addressed.

4.2. The virgin magnetization curve

Similar loops as those shown in Figure 3 were obtained for several temperatures, below and above the temperature of the steep increase of the coercive field when lowering T . We have found that the virgin curve excursion outside the regular loop takes place at low temperatures ($T \lesssim 20$ K) coinciding with the regime of SDWP described previously.

In some systems the virgin curve was observed to go outside the loop for a certain range of fields and temperatures [26, 27, 28, 29, 30, 31, 32]. In some complex magnetic oxides this feature was related with magnetic cation disorder [26, 27], which led not only to a spin-glass behavior but also to local structural distortions. These local distortions are due to a microscopic rearrangement of valence electrons [28], or to magnetic cations deficiency

¹This value was obtained considering the 010 direction as the easy magnetization axis

changing the nature of the local crystal field [29] which in turn lead to an irreversible movement of domain walls [28, 29]. The anomalous virgin curve in a ferrimagnet was also attributed to the development of an antiferromagnetic order at low temperature that produces a magnetic glass state [32].

Figure 5 shows the H derivative of the virgin curves dM/dH at several temperatures for the thin film, single crystals and polycrystalline pellets. In the thin film case (Figure 5(a)), the derivative is approximately constant. For all the other samples there is a maximum in the derivative that indicates a characteristic field, H_{max} , for the magnetic moments alignment, larger than the coercive field at low T (Figure 6).

In a spin glass scenario $H_{max}(T)$ could represent the line separating the glassy phase from the ordered state. Therefore a T dependence following the Almeida-Thouless [33] or Gabay-Toulouse [34] models could be expected. This is not our case, indicating a more complex behavior involving the hindering of DW movement. We have also ruled out the magnetic glass [16] scenario because we found no evidence for a long range antiferromagnetic order at low temperatures and we did not detect differences between FC cooling and FC warming magnetization measurements at 1 kOe as in a typical magnetic glass displaying the kinetic arrest of the phase transition [15]. The difference between H_{max} and H_c (Figure 6) is larger for single crystals than for polycrystalline pellets suggesting an intrinsic origin for this behavior.

4.3. The frustrated state and its removal

To understand the microscopic origin of the frustration the local magnetic interactions of Ni^{2+} have to be analyzed. They depend on the nearest magnetic neighbor (1 nnn) and on the exchange path for the second and third nearest neighbor (2 nnn, 3 nnn). Considering the structure (Figure 1(left)) with perfect stoichiometry and full Ni^{2+} occupancy of the $2d$ site, the interaction among 1 nnn relays on the presence of a Ni^{2+} in the closer $2c$ site (1/3 Ni^{2+} ion occupancy). If this is the case there will be an antiferromagnetic superexchange interaction of the Ni^{2+} -O- Ni^{2+} kind [10]. The remaining 2/3 of the $2c$ sublattice is occupied by non magnetic (d^{10}) Sb^{5+} ions. Then, a Ni^{2+} ferrimagnetic lattice is formed at the $2d$ and $2c$ sites. The $2d$ site Ni^{2+} second and third nearest neighbor interactions are mediated by -O-O- (at $\sim 90^\circ$) and -O- Sb^{5+} -O- (at $\sim 180^\circ$) super-superexchange paths (see Figure 1(right)), whose relative strength would determine the type of magnetic ordering in the regions with Sb^{5+} in the $2c$ sublattice. These super-superexchange interactions were found to be dominant for the antiferromagnetic structure of some

ordered double perovskites $A_2BB'O_6$ where B is a magnetic transition metal ion and B' is a non magnetic cation [35]. In particular, LaSrNiSbO_6 was found to have an antiferromagnetic structure of type I (ferromagnetic planes parallel to the ab and ac planes antiferromagnetically coupled along the c and b direction respectively) with a transition temperature of 26 K [36]. Therefore, for $\text{La}_2\text{Ni}(\text{Ni}_{1/3}\text{Sb}_{2/3})\text{O}_6$, at temperatures around 20 K, the Ni_{2d}^{2+} - Ni_{2d}^{2+} interactions mediated through -O-O- paths and the ones mediated through -O-Sb⁵⁺-O-, both antiferromagnetic in nature, became important. These interactions together with Ni^{2+} -O- Ni^{2+} superexchange one that exists below 100 K, create a magnetically frustrated state at lower temperatures than 20 K. A similar antiferromagnetic transition temperature was found in related Co based perovskites [37] and in $\text{La}_2\text{Ni}(\text{Ni}_{1/3}\text{Nb}_{2/3})\text{O}_6$ ². Consequently, a magnetically frustrated ground state is expected when cooling the sample in zero field due to competing antiferromagnetic interactions among the Ni^{2+} ions and H_{max} is necessary to overcome this frustration. The microscopic origin of the barrier which is overcome by increasing H at low T is still not clear. It is probably related to the spin orientation of the Ni^{2+} moments interacting antiferromagnetically with its 1 nnn trying to keep their antiferromagnetic arrangement in planes perpendicular to H and the uncompensated Ni^{2+} moments following the field as in a normal ferromagnet. The random orientation of the antiferromagnetic regions and the frustrated interaction near Sb^{5+} ions hinders the initial movement of the DW. When they are oriented, further changes of the magnitude of H result only in canting of the moments. However, the canting is not very important since a magnetization saturation value seems to be almost achieved at 5 T with M_s corresponding to the uncompensated Ni^{2+} moments in the ferrimagnetic structure, as described in previous sections. This model can be tested going back to the zero magnetization state with a demagnetizing protocol, illustrated in the insets of Figure 7. After this demagnetizing procedure, the zero magnetization state would involve only a random orientation of the uncompensated Ni^{2+} moments and the antiferromagnetically arranged regions would have the moments perpendicular to the direction of the preexisting field, providing a new ground state. Indeed, the results indicate that after this demagnetizing process, the sample initial magnetization branch lies inside the hysteresis loop.

² $\text{La}_2\text{Ni}(\text{Ni}_{1/3}\text{Nb}_{2/3})\text{O}_6$ shows an antiferromagnetic ordering at 28 K and is currently under study.

This is illustrated in Figure 7 for a single crystal at $T = 2$ K, where the virgin magnetization, the regular loop branch and a new initial magnetization branch are shown. This new initial magnetization is measured after the demagnetizing protocol shown in the inset.

The absence of exchange bias [21] in the magnetization loops indicate that large clusters with only antiferromagnetic super exchange Ni^{2+} -O- Ni^{2+} interactions are not likely to exist (i.e: the one third Ni^{2+} occupancy of the $2c$ site seems to be homogeneous at a microscopic level).

Figure 8 shows the comparison between the derivatives of the virgin curves and the initial magnetization after a demagnetizing protocol at 2 K for a single crystal and a polycrystalline pellet. We performed similar experiments at 5 and 10 K. In all the cases the new initial magnetization lies inside the loop as in a usual, non- frustrated, ferromagnet.

We can observe in Figure 8 that the initial susceptibility of the virgin curve after isothermal demagnetization is larger than the corresponding to the thermally demagnetized sample indicating that the new ground state is easier to magnetize in the direction of the preexisting magnetic field.

For the thin films, no indication of the frustrated state was found (Figures 3(a) and 5(a)). The superexchange and super-superexchange interactions are very sensitive to bond angles and lengths [11], which are likely modified near the surface. In our samples, the magnetic anisotropy imposed by the geometry seems to overcome the disordered interactions that sets in at low temperatures.

5. Conclusions

It is shown that the anomalous behavior of the virgin curve in hysteresis loops is a distinctive feature of a low temperature magnetic frustrated state found in the ferrimagnetic double perovskite oxide $\text{La}_2\text{Ni}(\text{Ni}_{1/3}\text{Sb}_{2/3})\text{O}_6$. The virgin curve lies outside the loops at $T \lesssim 20$ K, at about one fifth of the ferrimagnetic ordering temperature ($T_c \approx 100$ K). This was found to be an indication of a microscopically irreversible process possibly involving the interplay of antiferromagnetic interactions that hinder the initial movement of domain walls. This feature was observed in single crystals and in polycrystalline pelletized samples but not in thin films. This initial frustrated magnetic state is overcome by applying a characteristic field. Above this field the material behaves macroscopically as a typical ferromagnet. The model proposed for the frustrated state is based on the competing antiferromagnetic interaction

between 1 nnn and 3 nnn (ie: $\text{Ni}^{2+}\text{-O-Ni}^{2+}$ and $\text{Ni}^{2+}\text{-O-Sb}^{5+}\text{-O-Ni}^{2+}$). This microscopic scenario for the frustrated state is tested by going back to the zero magnetization state at fixed low temperature applying a demagnetizing protocol.

6. Acknowledgments

We thank P. Pedrazzini for help with the crystal growth and E. De Biasi for fruitful suggestions. R.E.C., E.E.K., and G.N. are members of CONICET, Argentina. D.G.F. has a scholarship from CONICET, Argentina. Work partially supported by ANPCyT PICT07-00819, CONICET PIP11220090100448 and SeCTyP-UNCuyo 06/C381. R.E.C. thanks FONCYT (PICT2007 00303), CONICET (PIP 11220090100995) and SECYT-UNC (Res. 214/10) for financial support. E.E.K. thanks ANPCyT PICT2008-1731 for financial support.

References

- [1] H. Takagi and H. Y. Hwang, *Science* 327 (2010) 1601-1602.
- [2] I. Levin, L. A. Bendersky, J. P. Cline, R. S. Roth and T. A. Vanderah, *J. Solid State Chem.* 150 (2000) 43-61.
- [3] K. -I. Kobayashi, T. Kimura, Y. Tomioka, H. Sawada, K. Terakura and Y. Tokura, *Phys. Rev. B* 59 (1999) 11159-11162.
- [4] K. L. Holman, Q. Huang, T. Klimczuk, K. Trzebiatowski, J. W. G. Bos, E. Morosan, J. W. Lynn and R. J. Cava, *J. Solid State Chem.* 180 (2007) 75-83.
- [5] H. -J. Koo and M. -H. Whangbo, *Inorg. Chem.* 45 (2006) 4440-4447.
- [6] M. C. Viola, M. S. Augsburger, R. M. Pinacca, J. C. Pedregosa, R. E. Carbonio and R. C. Mercader, *J. Solid State Chem.* 175 (2003) 252-257.
- [7] A. Maignan, B. Raveau, C. Martin and M. J. Hervieu, *J. Solid State Chem.* 144 (1999) 224-227.
- [8] S. H. Kim and P. D. Battle, *J. Solid State Chem.* 114 (1995) 174-183.
- [9] P. S. R. Murthy, K. R. Priolkar, P. A. Bhoje, A. Das, P. R. Sarode and A. K. Nigam, *J. of Magn. and Magn. Mater.* 322 (2010) 3704-3709.

- [10] J. B. Goodenough, *Magnetism and the Chemical Bond* (Interscience, New York. N.Y. 1993).
- [11] P. J. Hay, J. C. Thibeault and R. J. Hoffmann, *J. Am. Chem. Soc.* 97 (1975) 4884-4899.
- [12] P. R. Levstein, H. M. Pastawski and J. L. D'Amato, *J. Phys.: Condens. Matter* 2 (1990) 1781-1794.
- [13] D. Serrate, J. M. De Teresa and M. R. Ibarra, *J. Phys.: Condens. Matter* 19 (2007) 023201; and references therein.
- [14] X. -G. Li, X. J. Fan, G. Ji, W. B. Wu, K. H. Wong, C. L. Choy and H. C. Ku, *J. Appl. Phys.* 85 (1999) 1663-1666.
- [15] T. Sarkar, V. Pralong and B. Raveau, *Phys. Rev. B* 83 (2011) 214428.
- [16] S. B. Roy, P. Chaddah, V. K. Pecharsky and K. A. Gschneidner Jr., *Acta Materialia* 56 (2008) 5895-5906.
- [17] I. Alvarez, M. L. Veiga and C. Pico, *Solid State Ionics* 91 (1996) 265-271.
- [18] I. Alvarez, M. L. Veiga and C. Pico, *J. Alloys and Compd.* 255 (1997) 74-78.
- [19] D. G. Franco, R. E. Carbonio and G. Nieva "Change in the magnetic domain alignment process at the onset of a frustrated magnetic state in ferromagnetic $\text{La}_2\text{Ni}(\text{Ni}_{1/3}\text{Sb}_{2/3})\text{O}_6$ double perovskite" arXiv:1303.1372 [cond-mat.mtrl-sci] 2013.
- [20] J. Rodriguez-Carvajal, *Physica B* 192 (1993) 55-69.
- [21] J. Nogués and I. K. Schuller, *J. of Magn. and Magn. Mater.* 192 (1999) 203-232.
- [22] R. M. Pinacca, M. C. Viola, J.A. Alonso, J. C. Pedregosa and R. E. Carbonio, *J. Mater. Chem.* 15 (2005) 4648-4653.
- [23] M. C. Viola, J. A. Alonso, J. C. Pedregosa and R. E. Carbonio, *Eur. J. Inorg. Chem.* (2005) 1559-1564.
- [24] B. D. Cullity, *Introduction to Magnetic Materials* (Addison-Wesley, Reading, MA, 1972).

- [25] L. B. Steren, M. Sirena and J. Guimpel, *Phys. Rev. B* 65 (2002) 094431.
- [26] G. Alejandro, D. G. Lamas, L. B. Steren, J. E. Gayone, G. Zampieri, A. Caneiro, M. T. Causa and M. Tovar, *Phys. Rev. B* 67 (2003) 064424.
- [27] L. B. Morales, R. Zysler and A. Caneiro, *J. of Solid State Chemistry* 181 (2008) 1824-1832.
- [28] P. A. Joy and S. K. Date, *J. of Magn. and Magn. Mater.* 210 (2000) 31-34.
- [29] T. Sarkar, V. Duffort, V. Pralong, V. Caignaert and B. Raveau, *Phys. Rev. B* 83 (2011) 094409.
- [30] R. D. Zysler, D. Fiorani and A. M. Testa, *J. Magn. Magn. Mater.* 224 (2001) 5-11.
- [31] S. Senoussi, *J. Physique* 45 (1984) 315-322.
- [32] S. Patankar, S. K. Pandey, V. R. Reddy, A. Gupta, A. Banerjee and P. Chaddah, *EPL* 90 (2010) 57007.
- [33] J. R. L. de Almeida and D. J. Thouless, *J. Phys. A* 11 (1978) 983-990.
- [34] M. Gabay and G. Toulouse, *Phys. Rev. Lett.* 47 (1981) 201-204.
- [35] E. Rodríguez, M. L. López, J. Campo, M. L. Veiga and C. Pico, *J. Mater. Chem.* 12 (2002) 2798-2802.
- [36] M. P. Attfield, P. D. Battle, S. K. Bollen, T. C. Gibb and R. J. Whitehead, *J. Solid State Chem.* 100 (1992) 37-48.
- [37] V. C. Fuertes, M. C. Blanco, D. G. Franco, J. M. de Paoli, R. D. Sánchez and R. E. Carbonio, *Mater. Res. Bull.* 46 (2011) 62-69.

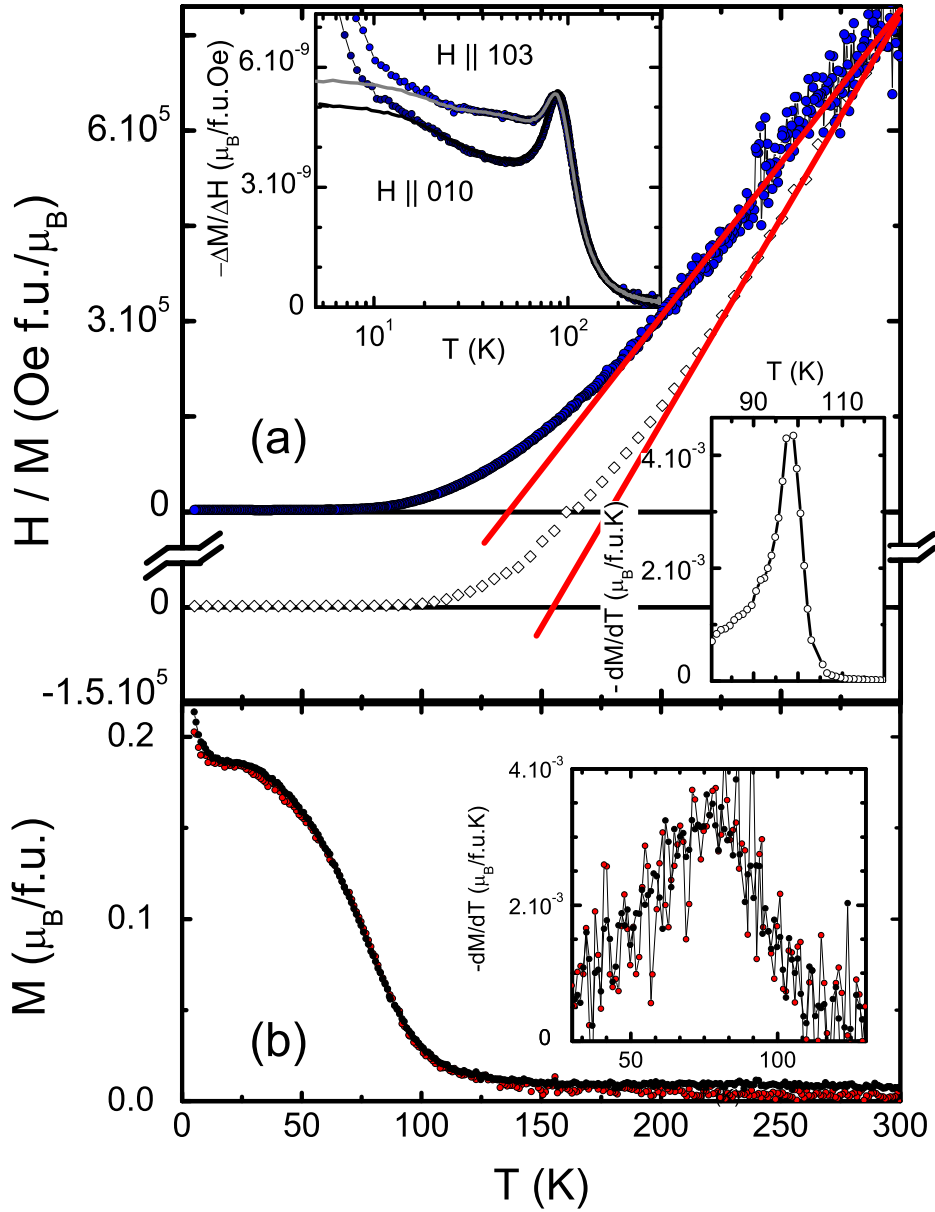


Figure 2: (color online) (a) H/M vs T for a single crystalline (solid symbols) and a polycrystalline (lower curve, open symbols) $\text{La}_2\text{Ni}(\text{Ni}_{1/3}\text{Sb}_{2/3})\text{O}_6$ samples, measured at 1000 Oe. The upper inset shows the susceptibility (defined in the text), $\Delta M/\Delta H$ vs T for H along (103) and (010) directions in the single crystal. The symbols indicate the ZFC and the line the FC measurement. The lower inset shows the magnetization derivative dM/dT vs T for a polycrystalline sample taken from a FC measurement at 1 Oe. (b) M vs T for two thin films of $\text{La}_2\text{Ni}(\text{Ni}_{1/3}\text{Sb}_{2/3})\text{O}_6$, measured at 1000 Oe. The inset shows dM/dT vs T for the same films FC measurement at 1000 Oe.

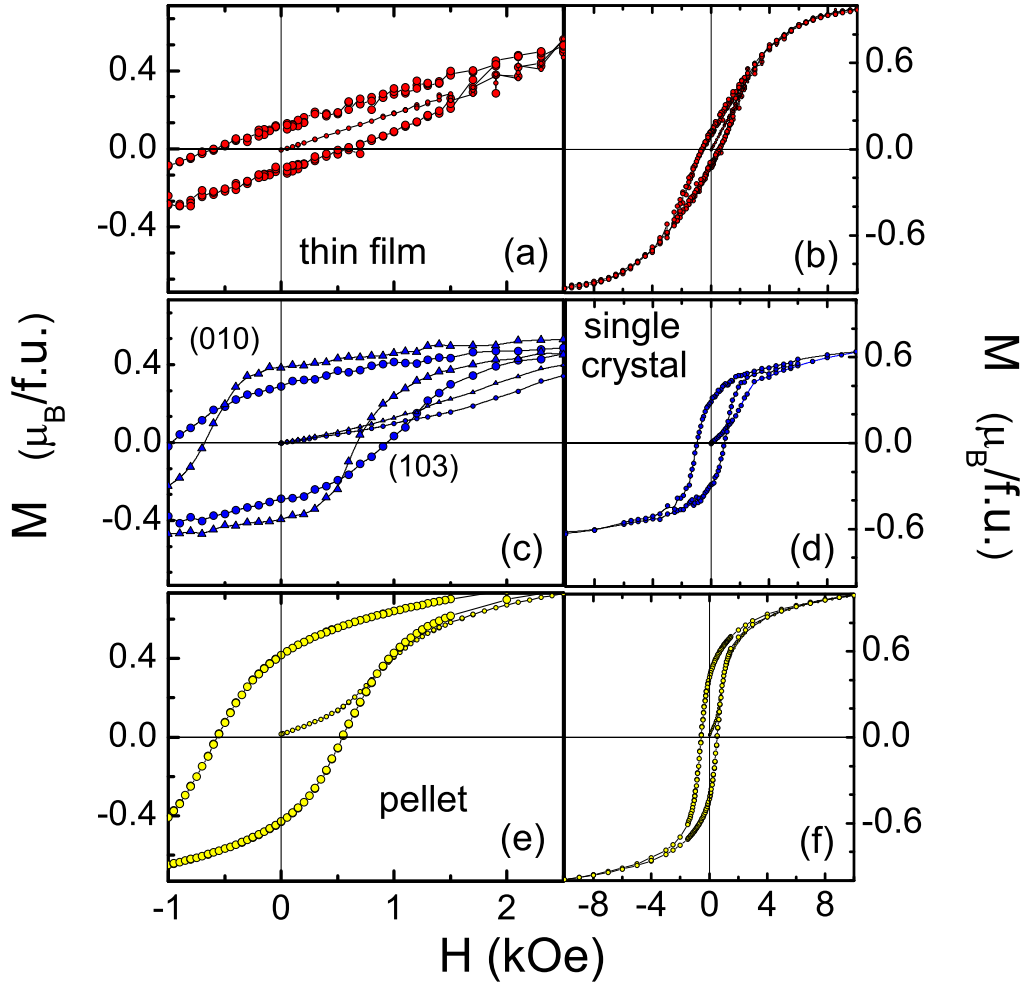


Figure 3: (color online) M vs H at 2 K for a thin film (a) and (b), a single crystal (c) and (d) and a polycrystalline pellet (e) and (f) of $\text{La}_2\text{Ni}(\text{Ni}_{1/3}\text{Sb}_{2/3})\text{O}_6$. For the single crystal(c), loops with the applied field along directions (103) and (010) are included.

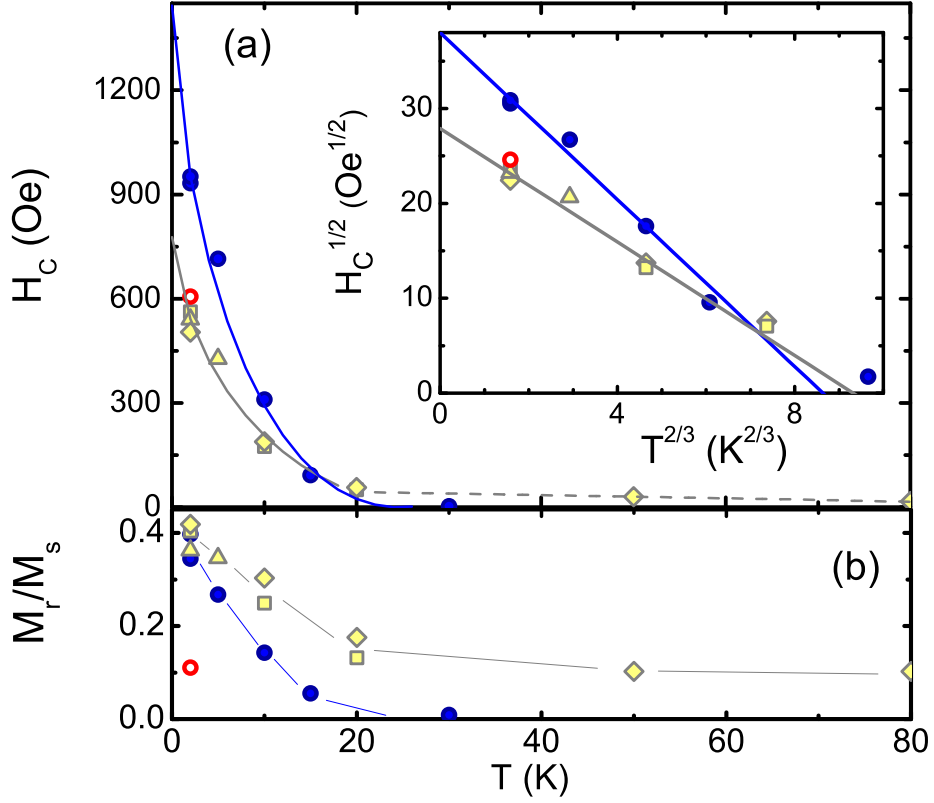


Figure 4: (color online) (a) Coercive field H_c vs T for $\text{La}_2\text{Ni}(\text{Ni}_{1/3}\text{Sb}_{2/3})\text{O}_6$ polycrystalline pellets (yellow, open symbols), single crystals (blue, dark circles) and thin films (open circles). The lines corresponds to models described in the text (SDWP and WDWP models, full lines and dashed line respectively). Inset: $H_c^{1/2}$ vs $T^{2/3}$ showing the linear behavior expected in the SDWP model. (b) Normalized remanent magnetization (at $H=0$) vs T , the symbols represent the same samples indicated in (a). The lines are a guide to the eye.

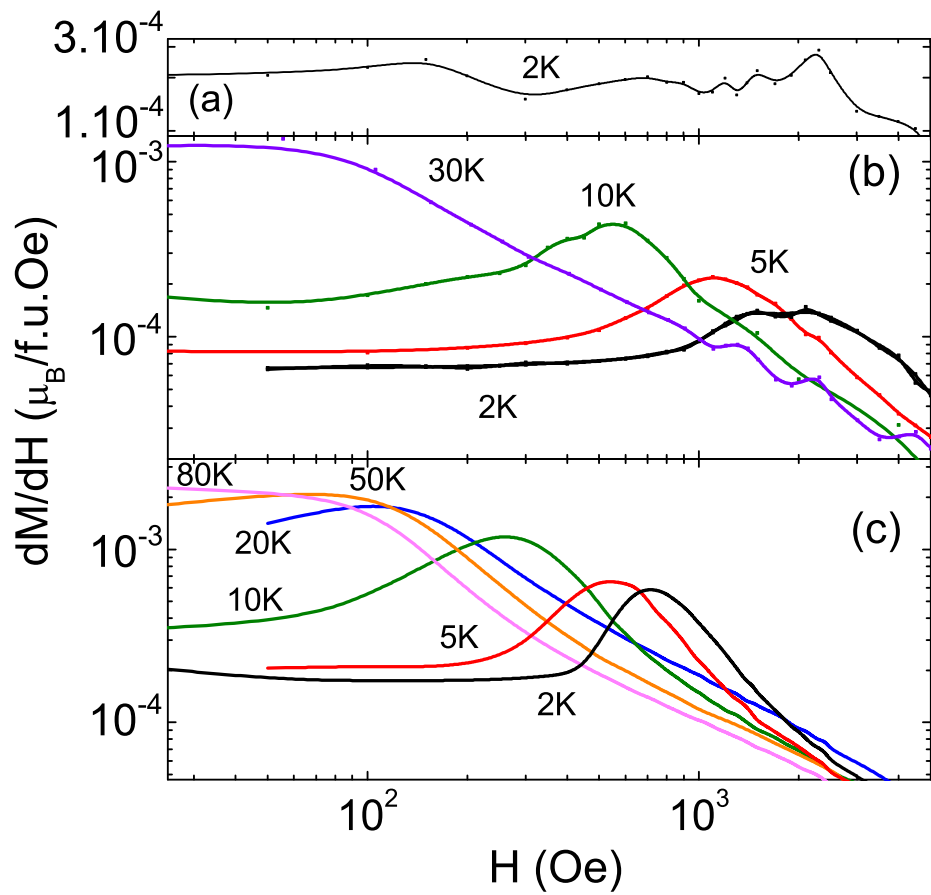


Figure 5: (color online) Derivative of the virgin curves in Magnetization loops for (a) thin film, (b) single crystals and (c) polycrystalline pellets.

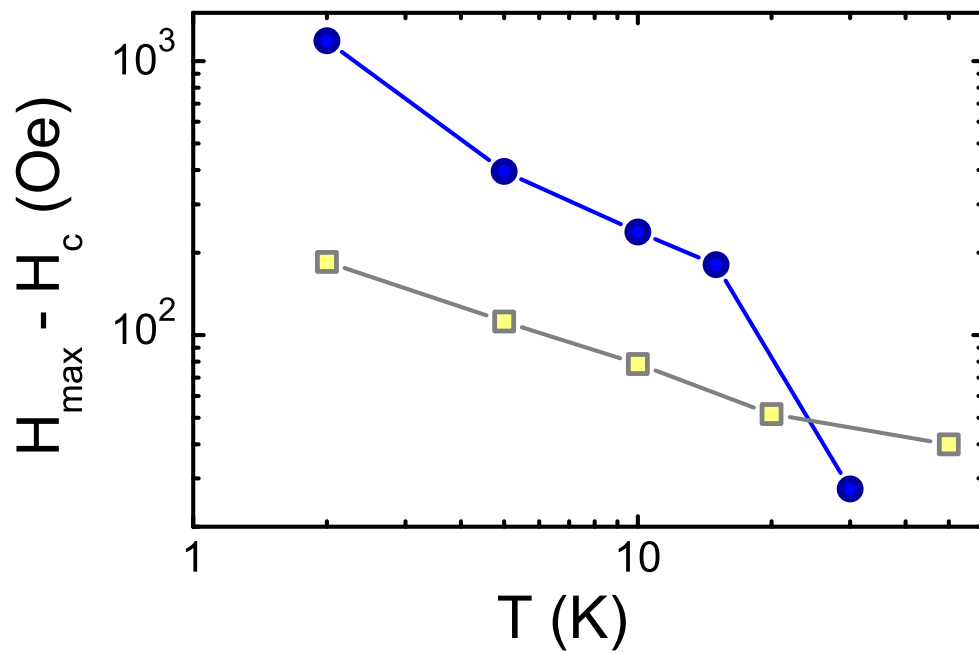


Figure 6: (color online) Difference of the field of the maximum slope of virgin curves in magnetization loops and the coercive field for crystals (blue, dark circles) and polycrystalline pellets (yellow, open squares). The lines are guide to the eye.

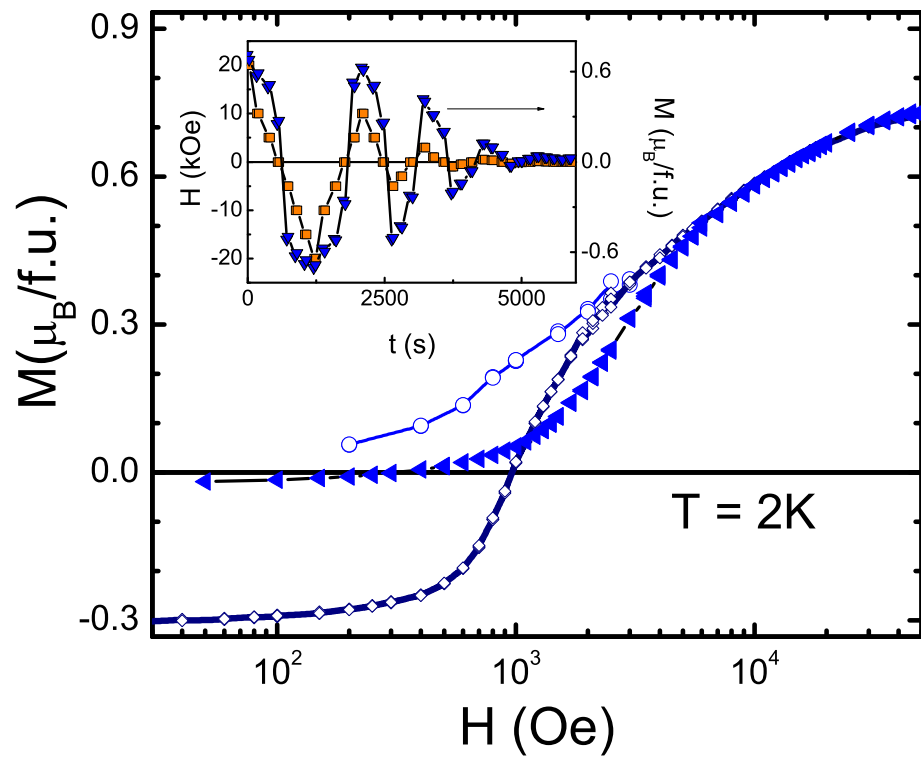


Figure 7: (color online) M vs H for a single crystalline sample at 2K showing the initial branch after a demagnetizing process (circles). The virgin curve (triangles) and the regular loop ascending field branch (diamonds) are also shown. Inset: M and H vs time in a demagnetizing process.

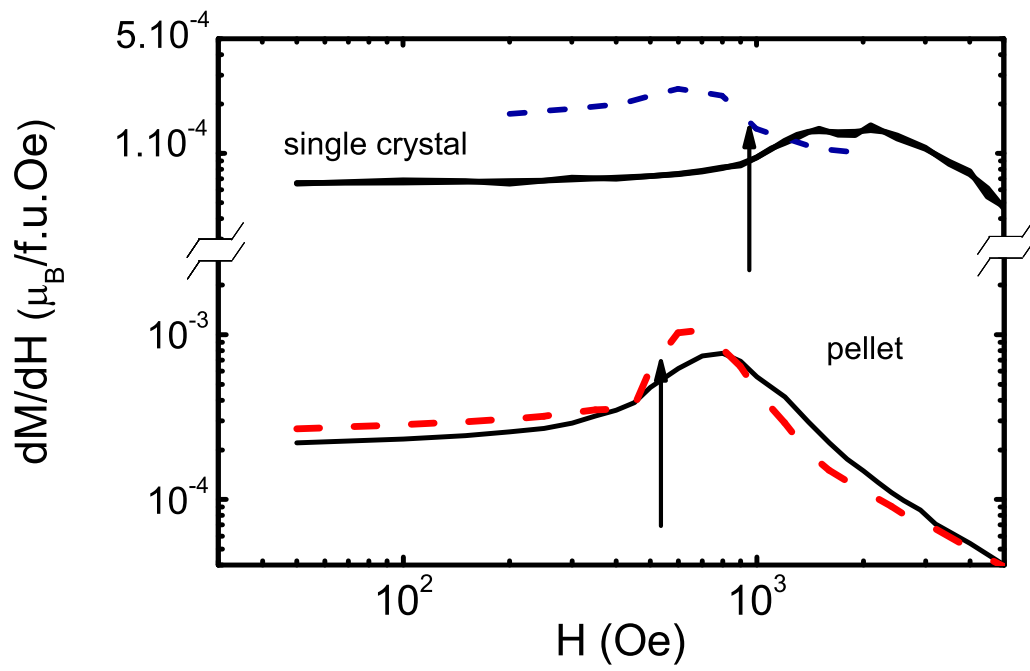


Figure 8: (color online) Comparison of the derivatives of the virgin curves in magnetization loops and the initial magnetization after a demagnetizing process, for a single crystal(a), a polycrystalline pellet (b). All the curves were taken at 2K. The arrows indicate the corresponding coercive field